

# Enhancing Diversity of OFDM with Joint Spread Spectrum and Subcarrier Index Modulations

Vu-Duc Ngo, Thien Van Luong, Nguyen Cong Luong, Mai Xuan Trang, Minh-Tuan Le, Thi Thanh Huyen Le, and Xuan-Nam Tran

**Abstract**—This paper proposes a novel spread spectrum and sub-carrier index modulation (SS-SIM) scheme, which is integrated to orthogonal frequency division multiplexing (OFDM) framework to enhance the diversity over the conventional IM schemes. Particularly, the resulting scheme, called SS-SIM-OFDM, jointly employs both spread spectrum and sub-carrier index modulations to form a precoding vector which is then used to spread an  $M$ -ary complex symbol across all active sub-carriers. As a result, the proposed scheme enables a novel transmission of three signal domains: SS and sub-carrier indices, and a single  $M$ -ary symbol. For practical implementations, two reduced-complexity near-optimal detectors are proposed, which have complexities less depending on the  $M$ -ary modulation size. Then, the bit error probability and its upper bound are analyzed to gain an insight into the diversity gain, which is shown to be strongly affected by the order of sub-carrier indices. Based on this observation, we propose two novel sub-carrier index mapping methods, which significantly increase the diversity gain of SS-SIM-OFDM. Finally, simulation results show that our scheme achieves better error performance than the benchmarks at the cost of lower spectral efficiency compared to classical OFDM and OFDM-IM, which can carry multiple  $M$ -ary symbols.

**Index Terms**—OFDM-IM, SS-SIM, spread spectrum, index modulation, spreading, precoding, Zadoff-Chu, detection designs.

## I. INTRODUCTION

Index modulation (IM) [1] has recently emerged as a promising modulation that exploits the indices of active sub-channels such as antennas [2], spreading codes [3] or sub-carriers [4] to carry additional data bits without requiring extra power or bandwidth. Therefore, IM not only exhibits higher reliability and energy efficiency (EE), but also lower complexity than conventional modulation schemes. Furthermore, it can enjoy an attractive trade-off between the spectral efficiency (SE) and the EE just by adjusting the number of active sub-channels. This makes IM a competitive candidate for machine type communications (MTC) [5], which require a high flexibility in terms of reliability, data rate and complexity.

The IM concept was first introduced to the orthogonal frequency division multiplexing (OFDM) in [4], and was then comprehensively analyzed in [6]. The resulting scheme,

termed as OFDM-IM, activates only a subset of sub-carriers to convey data bits via both the active indices and conventional  $M$ -ary symbols. Subsequently, a variety of IM techniques have been studied, which can be found in the survey [1]. For example, the analyses of the bit error rate (BER), achievable rate, and outage performance of OFDM-IM were presented in [7]–[9], respectively. Additionally, a number of studies aimed to improve the SE of OFDM-IM can be found in [10]–[13], in which extra bits are carried via additional signal domains, such as the index activation of inphase/quadrature (I/Q) components [10], subcarriers' constellation modes [11], [12] and 3-D constellation symbols [13]. In [14], noncoherent OFDM-IM was proposed, which conveys information only via the indices of active antennas, and thus, its signal detection does not require any channel state information (CSI). Then, a number of techniques were proposed to improve the SE of noncoherent OFDM-IM to be larger than 1 bps/Hz, such as deep learning (DL) [15] and multi-level index modulation [16]. Furthermore, the IM concept was utilized in other multicarrier waveforms such as orthogonal time frequency space (OTFS) modulation [17] and filter bank OFDM [18] in order to effectively combat Doppler effects in high-mobility channels and to reduce out-of-band emission (OOB), respectively. Recently, DL with deep neural networks (DNN) has also been applied to OFDM-IM as well as multicarrier systems in general. For instance, a deep learning-based detector for OFDM-IM called DeepIM was proposed in [19], which achieves a near-optimal performance at even lower runtime complexity than the energy-based greedy detector [7], followed by its reduced complexity version based on convolutional neural network (CNN) [20]. More specifically, a DNN architecture called autoencoder was developed for jointing representing and optimizing both transmitter and receiver of optical/wireless multicarrier OFDM-based systems in [21]–[24]. In other context, in [25], OFDM-IM is combined with multi-input multi-output (MIMO) systems, while in [26], [27] it is combined with both diversity receptions and greedy detection. Next, we will discuss the methods for improving the diversity of OFDM-IM without relying additional hardware such as antennas.

As inherited from classical OFDM, the performance of OFDM-IM is poor under a fading channel environment. To improve the reliability, a range of transmit diversity schemes have been proposed for OFDM-IM, without using multiple antennas. For instance, in [28], coordinate interleaved OFDM-IM (CI-OFDM-IM) was proposed to transmit real and imaginary parts of  $M$ -ary symbols via different sub-carriers, achieving a diversity gain of two. In [29], a linear constellation precoder was designed for OFDM-IM, also providing a diversity order

V.-D. Ngo is with the School of Electrical and Electronics Engineering, Hanoi University of Science and Technology, Hanoi 11657, Vietnam, (email: duc.ngovu@hust.edu.vn).

T. V. Luong, N. C. Luong, M. X. Trang are with the Faculty of Computer Science, Phenikaa University, Hanoi 12116, Vietnam (e-mail: {thien.luongvan, luong.nguyencong, trang.maixuan}@phenikaa-uni.edu.vn).

M.-T. Le is with the MobiFone R&D Center, MobiFone Corporation, Hanoi 11312, Vietnam, (e-mail: tuan.minh@mobifone.vn).

X.-N. Tran and T. T. H. Le are with the Advanced Wireless Communications Group, Le Quy Don Technical University, Ha Noi 11355, Vietnam (e-mail: {namtx, huyen.ltt}@mta.edu.vn).

of two. The repeated multicarrier index keying OFDM (MCIK-OFDM) was proposed in [30] to carry the same  $M$ -ary symbol over all active sub-carriers. The resulting scheme, termed as ReMO, increases the diversity gain up to two at the expense of the SE. Note that the terms of MCIK-OFDM and OFDM-IM are equivalent. Meanwhile, the repetition code for sub-carrier index (SI) symbols was presented in [31], combining with channel coding for  $M$ -ary symbols. A similar index repetition method for CI-OFDM-IM was reported in [32]. In [33], IM was applied to spread spectrum OFDM (SS-OFDM), where the indices of spreading codes are utilized to carry extra data bits and the resulting scheme is called SS-OFDM-IM. The spread matrices were applied to OFDM-IM in [34] to enhance its diversity gain at the cost of higher receiver complexity. In [35], the discrete Fourier transform (DFT) was applied to OFDM-IM to either improve its error performance or reduce its peak-to-average power ratio (PAPR) as well as OOB.

Note that most of the aforementioned schemes exploit only two signal dimensions including  $M$ -ary symbols and either sub-carrier indices or spreading code indices to offer the diversity gain limited by two. In this work, we propose a novel IM scheme which exploits all possible three IM signal dimensions, while achieving the diversity gain of even more than two. Our contributions are summarized as follows.

- A novel spread spectrum and sub-carrier index modulation for OFDM (SS-SIM-OFDM) is proposed, which jointly exploits SS and SI modulations to create a precoding matrix, which is then used to spread an  $M$ -ary complex symbol across all active sub-carriers. Interestingly, SS-SIM-OFDM not only forms a new transmission of three domains including SS and sub-carrier indices, and  $M$ -ary symbols, but also improves diversity gain over existing IM schemes with two signal domains [30], [33].
- We design two low-complexity detectors, namely the near-maximum likelihood (near-ML) and log-likelihood ratio-maximal ratio combining (LLR-MRC) detectors, whose complexities are shown to be less depending on the  $M$ -ary modulation size. Particularly, LLR-MRC separately detects sub-carrier indices and other signal domains, thus has much lower complexity than the near-ML detector at the cost of a slight performance loss.
- Based on the bit error probability (BEP) analysis, we discover that unlike existing IM schemes, the diversity gain of the proposed scheme is strongly influenced by the order of sub-carrier indices in each active SI set. This prompts us to propose two novel SI mapping methods to significantly enhance diversity gain of SS-SIM-OFDM.
- Simulations are carried out to verify the superior BEP of SS-SIM-OFDM over benchmark schemes, as well as the effectiveness of proposed diversity enhancement methods and reduced-complexity detectors.

The rest of this paper is organized as follows. Section II presents the system model, while Section III proposes two low-complexity detectors. The BEP analysis and diversity enhancement are reported in Section IV. In Section V, simulation results are provided. Finally, Section VI concludes the paper.

*Notation:* Upper-case bold and lower-case bold letters

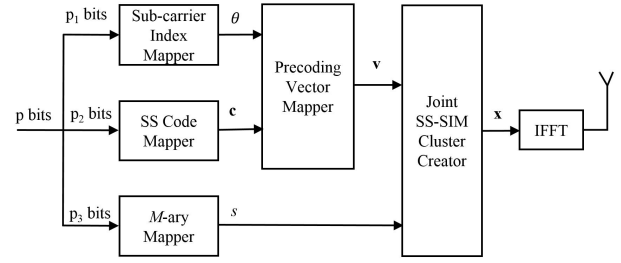


Fig. 1. Block diagram of one cluster of SS-SIM-OFDM.

present matrices and vectors, respectively.  $(\cdot)^T$  and  $(\cdot)^H$  stand for the transpose and Hermitian operations, respectively.  $\|\cdot\|$  denotes the Frobenious norm.  $\mathcal{CN}(0, \sigma^2)$  represents the complex Gaussian distribution with zero mean and variance  $\sigma^2$ . The ring of complex number, the binomial coefficient and the floor function are denoted by  $\mathbb{C}$ ,  $C(\cdot, \cdot)$  and  $\lfloor \cdot \rfloor$ , respectively.  $j$  is the unit imaginary number. The greatest common divisor of two integers is denoted by  $\gcd(\cdot, \cdot)$ .

## II. SYSTEM MODEL

Consider an SS-SIM-OFDM with  $N_c$  sub-carriers, which are divided into  $G$  clusters and each cluster has  $N$  sub-carriers, where  $N_c = GN$ . Without loss of generality, we only consider one cluster for simplicity. A block diagram of one SS-SIM-OFDM cluster is illustrated in Fig. 1. Unlike exiting IM schemes which carry information mainly via only two signal dimensions [1], the proposed SS-SIM-OFDM activates  $K$  out of  $N$  sub-carriers in every transmission per cluster to convey data bits through three signal domains as follows.

For each transmission in one cluster,  $p$  incoming bits are partitioned into three bit streams of  $p_1$ ,  $p_2$  and  $p_3$  bits, where  $p = p_1 + p_2 + p_3$ . The first stream of  $p_1$  bits are mapped into the set of  $K$  indices of active sub-carriers, which is denoted by  $\theta = \{\alpha_1, \dots, \alpha_K\}$ , where  $\alpha_k \in \{1, 2, \dots, N\}$  for  $k = 1, \dots, K$ . Here,  $\theta$  is referred to as a sub-carrier index (SI) symbol. The second stream of  $p_2$  bits are fed to the SS code mapper to determine the spreading code  $\mathbf{c} = [c_1, \dots, c_K]^T \in \mathcal{C} \subseteq \mathbb{C}^{K \times 1}$ , where  $\mathcal{C} = \{\mathbf{c}_1, \dots, \mathbf{c}_K\}$  is the set of  $K$  orthogonal codes.<sup>1</sup> The design of spreading codes will be discussed afterwards. Then, the precoding vector mapper utilizes  $\theta$  and  $\mathbf{c}$  to form the precoding vector  $\mathbf{v} = [v_1, \dots, v_N]^T$ , where  $v_\alpha = c_k$  for  $\alpha = \alpha_k \in \theta$ ,  $k = 1, \dots, K$  and  $v_\alpha = 0$  for  $\alpha \notin \theta$ . The precoding vector mapper is denoted by the function  $\mathbf{v} = \mathcal{T}(\theta, \mathbf{c})$ . For example, when  $N = 4$ ,  $K = 2$  and  $\theta = \{2, 3\}$ , we obtain  $\mathbf{v} = [0, c_1, c_2, 0]^T$ . The remaining  $p_3$  bits are mapped to an  $M$ -ary data symbol  $s \in \mathcal{S}$ , where  $\mathcal{S}$  denotes the  $M$ -ary modulation constellation. Finally, the transmitted signal in the frequency domain for each cluster is obtained by spreading this symbol across  $K$  active sub-carriers as follows  $\mathbf{x} = \mathbf{v}s$ .

The numbers of bits carried by sub-carrier and spreading code indices are  $p_1 = \lfloor \log_2 C(N, K) \rfloor$  and  $p_2 = \lfloor \log_2 K \rfloor$ ,

<sup>1</sup>Note that since we aim to spread the  $M$ -ary symbol over  $K$  active sub-carriers, the length of the spreading codes is equal to  $K$ .

respectively, while that of  $M$ -ary bits is  $p_3 = \log_2 M$ . Thus, the SE of SS-SIM-OFDM is given by

$$R = \frac{\lfloor \log_2 C(N, K) \rfloor + \lfloor \log_2 K \rfloor + \log_2 M}{N} \text{ (bps/Hz)}. \quad (1)$$

The received signal in the frequency domain is given by

$$\mathbf{y} = \mathbf{H}\mathbf{v}s + \mathbf{n} = \mathbf{H}\mathbf{x} + \mathbf{n}, \quad (2)$$

where  $\mathbf{H} = \text{diag}(h_1, \dots, h_N)$  denotes the Rayleigh fading channel matrix with  $h_n \sim \mathcal{CN}(0, 1)$  and  $\mathbf{n} \in \mathbb{C}^{N \times 1}$  is the additive white Gaussian noise vector with its elements  $\sim \mathcal{CN}(0, N_0)$ . Here, we assume the average receive signal-to-noise ratio (SNR) is  $\bar{\gamma} = 1/N_0$ . At the receiver, the transmitted signal can be detected by the maximum likelihood (ML) detector as follows:

$$(\hat{\theta}, \hat{\mathbf{c}}, \hat{s}) = \arg \min_{\theta, \mathbf{c}, s} \|\mathbf{y} - \mathbf{H}\mathbf{v}s\|^2. \quad (3)$$

This detector has a computational complexity of  $\mathcal{O}(2^p)$ , which is impractical when  $N$ ,  $K$  and  $M$  increase. Therefore, in Subsection III, we will design two low-complexity, near-optimal detectors for our SS-SIM-OFDM.

It is noteworthy that SS-SIM-OFDM jointly employs both SS and SI modulations, enabling a novel transmission of three signal domains, including the indices of subcarriers and spreading code, and the  $M$ -ary symbol. Hence, our scheme provides a higher SE than the IM schemes based on two signal domains only, such as ReMO [30] and SS-OFDM-IM [33], which transmit only a single  $M$ -ary symbol and an index symbol in either SI or SS domain. However, compared to classical OFDM and OFDM-IM, our scheme achieve lower SE for given values of  $N$ ,  $K$  and  $M$ , since these classical schemes can carry multiple  $M$ -ary symbols.<sup>2</sup> Additionally, the diversity gain of SS-SIM-OFDM can be notably enhanced, even to be higher than that of the existing IM schemes. This can be achieved through properly designing the SI mapper so that each  $M$ -ary data symbol or index symbol is conveyed involving as much different sub-carriers as possible, as will be shown in Section IV.

#### A. Designs of Spreading Codes

There are a number of well-known orthogonal spreading codes that can be used for SS-SIM-OFDM such as Walsh-Hadamard (WH) and Zadoff-Chu (ZC) codes. Notice from [33] that ZC not only offers better performance, but also has more flexible length than WH. More precisely, the length of ZC can be any positive integer, while that of WH must be an integer power of two. Consequently, we consider ZC for the proposed scheme.

In particular, the first ZC code is denoted by  $\mathbf{c}_1 = [c_1, \dots, c_K]^T$  which is given by

$$c_k = \begin{cases} e^{-\frac{j2\pi d}{K} \left( \frac{k^2}{2} + uk \right)} & \text{for even } K \\ e^{-\frac{j2\pi d}{K} \left[ \frac{k(k+1)}{2} + uk \right]} & \text{for odd } K \end{cases}, \quad (4)$$

<sup>2</sup>In our future work, we will attempt to increase the SE of the proposed scheme through conveying multiple  $M$ -ary symbols similar to OFDM-IM, while still ensuring the benefit of three signal domains.

where  $d$  is any integer relatively prime to  $K$ ,  $u$  is any integer and  $k = 1, \dots, K$ . Then, the  $k$ -th ZC code is determined as the  $k$ -th cyclically shifted version of  $\mathbf{c}_1$ . For instance,  $\mathbf{c}_2 = [c_K, c_1, \dots, c_{K-1}]^T$  and  $\mathbf{c}_3 = [c_{K-1}, c_K, \dots, c_{K-2}]^T$ . To further improve the performance, we propose to use the rotated ZC spreading codes which are defined by rotating each original ZC code  $\mathbf{c}_k$  by a dedicated angle of  $e^{\frac{j2\pi(k-1)}{B}}$  for  $k = 1, \dots, K$ , where  $B = MK - 1$ . It is worth noting that we choose  $B = MK - 1$  to maximize the diversity gain achieved in the SS index domain. This will be explained further in the performance analysis afterwards in Subsection IV.

### III. LOW COMPLEXITY RECEIVER DESIGNS

We propose two low-complexity detectors for SS-SIM-OFDM, namely the near-ML and log-likelihood ratio maximal ratio combining (LLR-MRC) detectors. The computational complexity analysis and comparison are also provided.

#### A. Near-ML Detector

Let us denote the set of SI symbols used for the SIM process as  $\mathcal{I} = \{\theta_1, \dots, \theta_{2^{p_1}}\}$ . The near-ML detector first fixes the SI symbol  $\theta_i \in \mathcal{I}$  to detect the corresponding spreading code  $\hat{\mathbf{c}}_i$  and  $M$ -ary symbol  $\hat{s}_i$  as follows. For a given vector  $\mathbf{u} = [u_1, \dots, u_N]^T \in \mathbb{C}^{N \times 1}$ , denote by  $\mathbf{u}(\theta)$  the  $K \times 1$  vector whose elements have the indices of  $\theta$ . For example, when  $(N, K) = (4, 2)$  and  $\theta = \{1, 3\}$ , we attain  $\mathbf{u}(\theta) = [u_1, u_3]^T$ . The same operation can be applied to the diagonal matrix such as  $\mathbf{U}(\theta) = \text{diag}(u_1, u_3)$ , where  $\mathbf{U} = \text{diag}(\mathbf{u})$ . Based on this definition, for each  $\theta_i \in \mathcal{I}$ , we extract  $\mathbf{H}_i = \mathbf{H}(\theta_i)$  and  $\mathbf{y}_i = \mathbf{y}(\theta_i)$ . Then, for each  $\mathbf{c}_k \in \mathcal{C}$  with  $k = 1, \dots, 2^{p_2}$ , the  $M$ -ary symbol  $s_{i,k}$  is estimated based on the MRC as

$$s_{i,k} = \mathcal{Q} \{ \mathbf{H}_{i,k}^H \mathbf{y}_i / W_i \}, \quad (5)$$

where  $\mathbf{H}_{i,k} = \mathbf{H}_i \mathbf{c}_k$ ,  $W_i = \|\mathbf{H}_i\|^2$  and  $\mathcal{Q}(s)$  represents the digital demodulator function that returns the  $M$ -ary symbol which is the closest one to  $s$ . The symbol  $s_{i,k}$  is then utilized to calculate the distance  $\Delta_{i,k} = \|\mathbf{y}_i - \mathbf{H}_{i,k} s_{i,k}\|^2$ . After obtaining  $2^{p_2}$  symbols  $s_{i,k}$  and distances  $\Delta_{i,k}$ , we can generate the best  $\hat{\mathbf{c}}_i$  and  $\hat{s}_i$  for each  $\theta_i$ , as follows

$$\hat{\mathbf{c}}_i = \mathbf{c}_{\hat{k}_i}, \quad \hat{s}_i = s_{i,\hat{k}_i}, \quad (6)$$

where  $\hat{k}_i = \arg \min_{k=1, \dots, 2^{p_2}} \Delta_{i,k}$ . We use (6) to compute the overall distance  $\Theta_i = \|\mathbf{y} - \mathbf{H}\mathbf{v}_i \hat{s}_i\|^2$ , where  $\mathbf{v}_i = \mathcal{T}(\theta_i, \hat{\mathbf{c}}_i)$ .

Finally, the transmitted signal is recovered based on the minimum distance out of  $2^{p_1}$  distances  $\Theta_i$ , as follows

$$\hat{\theta} = \theta_{\hat{i}}, \quad \hat{\mathbf{c}} = \hat{\mathbf{c}}_{\hat{i}}, \quad \hat{s} = \hat{s}_{\hat{i}}, \quad (7)$$

where  $\hat{i} = \arg \min_{i=1, \dots, 2^{p_1}} \Theta_i$ .

The proposed near-ML detector is summarized in Algorithm 1. Its main idea is that for given sub-carrier activation  $\theta_i$ , it extracts the corresponding active sub-channels  $\mathbf{H}_i$  in order to detect the corresponding spreading code and data symbol based on the minimum Euclidean distance criterion.

Since the near-ML detector only uses sub-channels, i.e.,  $\mathbf{H}_i$  and the MRC for detection of the spreading code and the  $M$ -ary symbol, its complexity can be considerably reduced compared to the ML in (3). Despite that, our near-ML still achieves the near-ML performance, as shown in Section V.

**Algorithm 1** Near-ML Detection Algorithm**Input:**  $\mathbf{y}$ ,  $\mathbf{H}$ ,  $\mathcal{C}$  and  $\mathcal{I}$ **Output:**  $\hat{\theta}$ ,  $\hat{\mathbf{c}}$  and  $\hat{s}$ 

- 1) **for**  $i = 1$  **to**  $2^{p_1}$  **do**
- 2) Extract  $\mathbf{H}_i = \mathbf{H}(\theta_i)$  and  $\mathbf{y}_i = \mathbf{y}(\theta_i)$ , where  $\theta_i \in \mathcal{I}$ .
- 3) Calculate  $W_i = \|\mathbf{H}_i\|^2$ .
- 4) **for**  $k = 1$  **to**  $2^{p_2}$  **do**
- 5) Calculate  $\mathbf{H}_{i,k} = \mathbf{H}_i \mathbf{c}_k$ , where  $\mathbf{c}_k \in \mathcal{C}$ .
- 6) Estimate  $s_{i,k} = \mathcal{Q}\left\{\frac{\mathbf{H}_{i,k}^H \mathbf{y}_i}{W_i}\right\} \in \mathcal{S}$ .
- 7) Compute  $\Delta_{i,k} = \|\mathbf{y}_i - \mathbf{H}_{i,k} s_{i,k}\|^2$ .
- 8) **end for**
- 9) Estimate  $\hat{k}_i = \arg \min_{k=1, \dots, 2^{p_2}} \Delta_{i,k}$ .
- 10) Generate  $\hat{\mathbf{c}}_i = \mathbf{c}_{\hat{k}_i}$  and  $\hat{s}_i = s_{i, \hat{k}_i}$ .
- 11) Compute  $\Theta_i = \|\mathbf{y} - \mathbf{H} \mathbf{v}_i \hat{s}_i\|^2$ , where  $\mathbf{v}_i = \mathcal{T}(\theta_i, \hat{\mathbf{c}}_i)$ .
- 12) **end for**
- 13) Estimate  $\hat{i} = \arg \min_{i=1, \dots, 2^{p_1}} \Theta_i$ .
- 14) Generate the output  $\hat{\theta} = \theta_{\hat{i}}$ ,  $\hat{\mathbf{c}} = \hat{\mathbf{c}}_{\hat{i}}$  and  $\hat{s} = \hat{s}_{\hat{i}}$ .

**B. LLR-MRC Detector**

In order to further reduce the complexity of the near-ML detector, we now propose the LLR-MRC detector which separately detects sub-carrier indices, and the symbols in the two remaining signal dimensions. Particularly, the LLR method is used to recover the indices of active sub-carriers first, and then both the spreading code and the  $M$ -ary symbol are estimated based on the MRC approach.

In the first step, for each sub-carrier  $n$ , the LLR [31] is computed by

$$\lambda_n = - \min_{m=1, \dots, M} r_m + |y_n|^2, \quad (8)$$

where  $r_m = |y_n - h_n x_m|^2$  with  $x_m \in \mathcal{S}$ , and  $y_n$  is the  $n$ -th element of  $\mathbf{y}$ . Notice that this ratio gives information about the activity status of the sub-carrier, i.e., the larger LLR means the corresponding sub-carrier is more likely to be active. Hence, the  $N$  LLRs are arranged in the descending order  $\lambda_{\alpha_1} \geq \dots \geq \lambda_{\alpha_N}$ , where  $\alpha_n \in \{1, \dots, N\}$  to decide  $\hat{\theta} = \{\alpha_1, \dots, \alpha_K\}$ , i.e., indices of  $K$  largest LLR values. However, such an SI detection may lead to the unexpected case of  $\hat{\theta} \notin \mathcal{I}$ . To tackle this, we can replace  $\alpha_K$  (the index of the smallest LLR in  $\hat{\theta}$ ) with  $\alpha_{K+1}$  (the index of the largest LLR not in  $\hat{\theta}$ ) to obtain new indices as  $\hat{\theta} = \{\alpha_1, \dots, \alpha_{K-1}, \alpha_{K+1}\}$ . In case the new  $\hat{\theta}$  is still not included in  $\mathcal{I}$ , we continue to replace  $\alpha_{K-1} \in \hat{\theta}$  with  $\alpha_{K+2} \notin \hat{\theta}$ . In fact, such the case rarely occurs, carrying out the replacement once is sufficient to improve the performance.

Next, utilizing  $\hat{\theta}$ , the MRC with the input of  $\hat{\mathbf{H}} = \mathbf{H}(\hat{\theta})$  and  $\hat{\mathbf{y}} = \mathbf{y}(\hat{\theta})$  is employed to decode both  $\hat{\mathbf{c}}$  and  $\hat{s}$ . This step is similar to the inner for-loop of Algorithm 1. Thus, it is omitted for brevity. The summary of LLR-MRC is given in Algorithm 2. It is worth noting that the LLR-MRC exhibits remarkably lower complexity than the near-ML detector at the cost of the performance loss, as analyzed in the next section.

**Algorithm 2** LLR-MRC Detection Algorithm**Input:**  $\mathbf{y}$ ,  $\mathbf{H}$ ,  $\mathcal{C}$  and  $\mathcal{I}$ **Output:**  $\hat{\theta}$ ,  $\hat{\mathbf{c}}$  and  $\hat{s}$ 

- 1) **for**  $n = 1$  **to**  $N$  **do**
- 2) Compute  $r_m = |y_n - h_n x_m|^2$ ,  $x_m \in \mathcal{S}$ ,  $m = 1, \dots, M$ .
- 3) Calculate LLR ratio  $\lambda_n = - \min_{m=1, \dots, M} r_m + |y_n|^2$ .
- 4) **end for**
- 5) Arrange  $N$  ratios in descending order  $\lambda_{\alpha_1} \geq \dots \geq \lambda_{\alpha_N}$ , where  $\alpha_n \in \{1, \dots, N\}$  to obtain  $\hat{\theta} = \{\alpha_1, \dots, \alpha_K\}$ .
- 6) **if**  $\hat{\theta} \notin \mathcal{I}$
- 7) Update new indices  $\hat{\theta} = \{\alpha_1, \dots, \alpha_{K-1}, \alpha_{K+1}\}$ .
- 8) **end if**
- 9) Extract  $\hat{\mathbf{H}} = \mathbf{H}(\hat{\theta})$  and  $\hat{\mathbf{y}} = \mathbf{y}(\hat{\theta})$ .
- 10) Calculate  $W = \|\hat{\mathbf{H}}\|^2$ .
- 11) **for**  $k = 1$  **to**  $2^{p_2}$  **do**
- 12) Calculate  $\hat{\mathbf{H}}_k = \hat{\mathbf{H}} \mathbf{c}_k$ , where  $\mathbf{c}_k \in \mathcal{C}$ .
- 13) Estimate  $s_k = \mathcal{Q}\left\{\frac{\hat{\mathbf{H}}_k^H \hat{\mathbf{y}}}{W}\right\} \in \mathcal{S}$ .
- 14) Compute  $\Delta_k = \|\hat{\mathbf{y}} - \hat{\mathbf{H}}_k s_k\|^2$ .
- 15) **end for**
- 16) Estimate  $\hat{k} = \arg \min_{k=1, \dots, 2^{p_2}} \Delta_k$ .
- 17) Generate the output  $\hat{s} = s_{\hat{k}}$  and  $\hat{\mathbf{c}} = \mathbf{c}_{\hat{k}}$ .

**C. Complexity Analysis and Comparison**

We evaluate the computational complexity of the near-ML, LLR-MRC and ML detectors by calculating the number of floating-point operations (flops) per sub-carrier. A flop can be a real addition, subtraction, division or multiplication. For example, a complex multiplication can be counted by 6 flops since it requires 2 real additions and 4 real multiplications, or the operation of  $|z|^2$  where  $z \in \mathbb{C}$  requires 3 flops corresponding to 2 real multiplications and 1 real addition.

Based on the definition of a flop, the numbers of flops required in steps 3, 5, 6, 7 and 11 of the near-ML detector are  $4K - 1 \approx 4K$ ,  $6K$ ,  $8K$ ,  $12K$  and  $14K + 5N$ , respectively. Notice that the complexity involved in the digital demodulator function  $\mathcal{Q}(\cdot)$  is negligible in comparison with other calculations. As a result, the number of flops per sub-carrier of the near-ML detector can be approximated by

$$C_{\text{near-ML}} \approx \frac{2^{p_1} [(26 \times 2^{p_2} + 18) K + 4N]}{N}. \quad (9)$$

Similarly, we attain the complexities of the LLR-MRC and ML detectors in terms of flops/sub-carrier, respectively, as follows

$$C_{\text{LLR-MRC}} \approx \frac{2^{p_2} \times 26K + 4K}{N} + 15, \quad (10)$$

$$C_{\text{ML}} \approx \frac{2^{p_1+p_2} (4N + 14K) M}{N}. \quad (11)$$

It is worth mentioning that unlike the ML, the complexities of both the proposed detectors are roughly independent of the  $M$ -ary modulation size, thus are significantly lower than that of the ML, especially when  $M$  increases. For this, we provide Fig. 2(a) and (b) to illustrate such a complexity reduction. It is clearly shown from Fig. 2 that the proposed

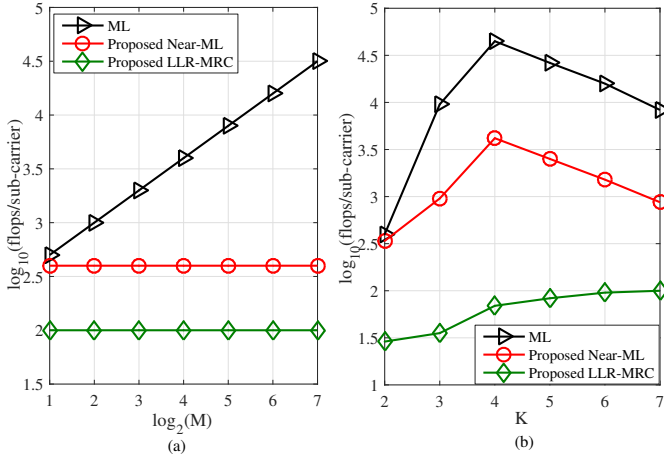


Fig. 2. Computational complexity comparisons between two proposed detectors and the ML detector when (a)  $N = 5, K = 4, M = 2, 4, \dots, 128$  and (b)  $N = 8, M = 16, K = 2, \dots, 7$ .

detectors offer the notably reduced complexity compared with the ML, especially the LLR-MRC detector. For instance, in Fig. 2(a), when  $(N, K, M) = (5, 4, 64)$ , the number of flops per sub-carrier of the ML detector is 15564, while that of the proposed near-ML and LLR-MRC detectors are 406 and 101, respectively. As a result, the near-ML and LLR-MRC detectors can save 97.4% and 99.3% complexity, respectively, with respect to the ML detector.

#### IV. PERFORMANCE ANALYSIS AND DIVERSITY ENHANCEMENT

We investigate the BEP of SS-SIM-OFDM with the ML detection. In particular, the pairwise error probability (PEP) is analyzed to gain an insight into the achievable diversity gain and the theoretical bound on the BEP. More importantly, based on the analysis, we find out two SI mapping methods which enhance the diversity order of SS-SIM-OFDM.

##### A. BEP Analysis

For given  $\mathbf{H}$ , the well-known conditional PEP of the pairwise error event (PEE) that the transmitted vector  $\mathbf{x}$  is incorrectly estimated as  $\hat{\mathbf{x}} \neq \mathbf{x}$ , is given by

$$P(\mathbf{x} \rightarrow \hat{\mathbf{x}}|\mathbf{H}) = Q\left(\sqrt{\frac{\|\mathbf{H}(\mathbf{v}\mathbf{s} - \hat{\mathbf{v}}\hat{\mathbf{s}})\|^2}{2N_0}}\right), \quad (12)$$

where we assume that  $\mathbf{x} = \mathbf{v}\mathbf{s}$  and  $\hat{\mathbf{x}} = \hat{\mathbf{v}}\hat{\mathbf{s}}$  with  $\mathbf{v} = \mathcal{T}(\theta, \mathbf{c})$  and  $\hat{\mathbf{v}} = \mathcal{T}(\hat{\theta}, \hat{\mathbf{c}})$ , and  $Q(\cdot)$  denotes the Gaussian tail probability [36]. Let us denote  $\mathbf{v} = [v_1, \dots, v_N]^T$ ,  $\hat{\mathbf{v}} = [\hat{v}_1, \dots, \hat{v}_N]^T$  and  $\beta_n = |v_n s - \hat{v}_n \hat{s}|^2$  for  $n = 1, \dots, N$ . We rewrite (12) as

$$P(\mathbf{x} \rightarrow \hat{\mathbf{x}}|\mathbf{H}) = Q\left(\sqrt{\frac{\sum_{n=1}^N \beta_n \gamma_n}{2}}\right), \quad (13)$$

where  $\gamma_n = |h_n|^2 / N_0 = \bar{\gamma} |h_n|^2$  is the instantaneous SNR of the  $n$ -th sub-carrier. Utilizing the approximation of  $Q(x) \approx e^{-x^2/2}/12 + e^{-2x^2/3}/4$  [36], we can approximate (13) as

$$P(\mathbf{x} \rightarrow \hat{\mathbf{x}}|\mathbf{H}) \approx \frac{1}{12}e^{-\frac{\Upsilon}{4}} + \frac{1}{4}e^{-\frac{\Upsilon}{3}}, \quad (14)$$

where  $\Upsilon = \sum_{n=1}^N \beta_n \gamma_n$ .

Since the Rayleigh channel model is assumed, we attain the moment generating function (MGF) of  $\eta_n = \beta_n \gamma_n$  as  $\mathcal{M}_{\eta_n}(t) = (1 - \beta_n \bar{\gamma} t)^{-1}$  for  $n = 1, \dots, N$ . Consequently, the MGF of  $\Upsilon = \sum_{n=1}^N \eta_n$  is given by  $\mathcal{M}_{\Upsilon}(t) = \prod_{n=1}^N \mathcal{M}_{\eta_n}(t) = \prod_{n=1}^N (1 - \beta_n \bar{\gamma} t)^{-1}$ . Applying the MGF approach to (14), the unconditional PEP is obtained as follows<sup>3</sup>

$$P(\mathbf{x} \rightarrow \hat{\mathbf{x}}) \approx \frac{1/12}{\prod_{n=1}^N \left(1 + \frac{\beta_n \bar{\gamma}}{4}\right)} + \frac{1/4}{\prod_{n=1}^N \left(1 + \frac{\beta_n \bar{\gamma}}{3}\right)}. \quad (15)$$

It can be seen from (15) that the diversity order of  $P(\mathbf{x} \rightarrow \hat{\mathbf{x}})$  is the number of non-zero elements  $\beta_n$ . Thus, letting  $d(\mathbf{x}, \hat{\mathbf{x}})$  be the number of non-zero elements of vector  $\mathbf{x} - \hat{\mathbf{x}}$ , the diversity order of SS-SIM-OFDM becomes

$$G_d = \min_{\mathbf{x} \neq \hat{\mathbf{x}}} d(\mathbf{x}, \hat{\mathbf{x}}), \quad (16)$$

which is the minimum value of the diversity orders of all the unconditional PEPs in (15).

To compute  $G_d$ , we investigate two main cases of the PEEs, taking the proposed rotated ZC codes into account as follows.

**Case 1**  $\theta = \hat{\theta}$ : Without loss of generality, we assume  $\theta = \hat{\theta} = \{1, 2, \dots, K\}$ , leading to  $\beta_n = 0$  for  $n > K$  and  $\beta_n = |c_n s - \hat{c}_n \hat{s}|^2$  for  $n = 1, \dots, K$ , where it is assumed that  $\mathbf{c} = [c_1, \dots, c_K]^T$  and  $\hat{\mathbf{c}} = [\hat{c}_1, \dots, \hat{c}_K]^T$ . As a result, we deduce  $d(\mathbf{x}, \hat{\mathbf{x}}) = d(\mathbf{c}\mathbf{s}, \hat{\mathbf{c}}\hat{\mathbf{s}}) \leq K$ , which results in three possible cases as follows.

If  $s = \hat{s}$  and  $\mathbf{c} \neq \hat{\mathbf{c}}$ , it is obtained that  $d(\mathbf{c}\mathbf{s}, \hat{\mathbf{c}}\hat{\mathbf{s}}) = d(\mathbf{c}, \hat{\mathbf{c}})$ . In case  $K$  is odd, according to (4), we assume that  $c_k = e^{j\varphi_1}$  and  $\hat{c}_k = e^{j\varphi_2}$  with  $\varphi_1 = -j\pi d(k_1^2 + k_1)/K + 2j\pi l_1/B$  and  $\varphi_2 = -j\pi d(k_2^2 + k_2)/K + 2j\pi l_2/B$ , where  $1 \leq k_1, k_2 \leq K$  and  $0 \leq l_1 < l_2 < K$ . Note that we choose  $u = 0$  in (4) to identify such  $c_k$  and  $\hat{c}_k$ . If  $c_k = \hat{c}_k$ , there exists  $q \in \mathbb{Z}$  such that  $\varphi_1 = j2\pi q + \varphi_2$ , which is equivalent to

$$2K(l_2 - l_1) = B[d(k_2^2 + k_2 - k_1^2 - k_1) - 2qK]. \quad (17)$$

Since  $\gcd(B, 2) = \gcd(B, K) = 1$ , we deduce from (17) that  $l_2 - l_1$  is a multiple of  $B$ . However, this clearly conflicts with  $0 < l_2 - l_1 < K < B$ . As a result,  $c_k \neq \hat{c}_k$  for every  $k = 1, \dots, K$  and thus  $d(\mathbf{x}, \hat{\mathbf{x}}) = d(\mathbf{c}, \hat{\mathbf{c}}) = K$ . It is worth noting that for even  $K$ , we arrive at the same conclusion.

If  $s \neq \hat{s}$  and  $\mathbf{c} \neq \hat{\mathbf{c}}$ , we assume  $s = e^{j2\pi m_1/M}$  and  $\hat{s} = e^{j2\pi m_2/M}$ ,  $0 \leq m_1 < m_2 < M$ , where the PSK modulation is used. If  $c_k s - \hat{c}_k \hat{s} = 0$ , similar to the first case, we deduce

$$B[d\Phi M - 2K(qM + m_2 - m_1)] = 2MK(l_2 - l_1), \quad (18)$$

where  $\Phi = k_2^2 + k_2 - k_1^2 - k_1$ . Due to the fact of  $\gcd(B, 2) = \gcd(B, MK) = 1$ , we attain  $l_2 - l_1$  which is a multiple of  $B$ . This is impossible since  $0 < l_2 - l_1 < B$ . Therefore,  $c_k s - \hat{c}_k \hat{s} \neq 0$  for every  $k = 1, \dots, K$ , leading to  $d(\mathbf{x}, \hat{\mathbf{x}}) = K$ .

In case of  $s \neq \hat{s}$  and  $\mathbf{c} = \hat{\mathbf{c}}$ , it is shown that  $\beta_k = |c_k s - \hat{c}_k \hat{s}|^2 = |c_k|^2 |s - \hat{s}|^2 \neq 0$  for every  $k = 1, \dots, K$ . Hence, the diversity order achieved in this case is still  $K$ .

<sup>3</sup>Note that our analysis here can be applied to any channel model, and hence is not limited to Rayleigh fading. In particular, for a new channel model such as Rician, we just need to apply the MGF of that channel to (14) for achieving the corresponding unconditional PEP. We leave such performance evaluation of our scheme over generalized fading channels as our future work.

*Remark 1.* In case of  $\theta = \hat{\theta}$ , thanks to the proposed rotated ZC codes, the diversity order of SS-SIM-OFDM is maximized to be  $K$ , i.e., the number of active sub-carriers in both the  $M$ -ary and SS index domains.

**Case 2  $\theta \neq \hat{\theta}$ :** There exists at least two sub-carrier indices  $n_1 \neq n_2 \in \{1, \dots, N\}$  such that  $v_{n_1} \neq 0$ ,  $\hat{v}_{n_1} = 0$  and  $v_{n_2} = 0$ ,  $\hat{v}_{n_2} \neq 0$ . As a consequence, we obtain  $\beta_{n_1} = |v_{n_1}s|^2 \neq 0$  and  $\beta_{n_2} = |\hat{v}_{n_2}\hat{s}|^2 \neq 0$ , which leads to  $d(\mathbf{x}, \hat{\mathbf{x}}) \geq 2$ . However, employing the conventional SI mapping methods such as the combinatorial method [6], there always exist two vectors  $\mathbf{x}$  and  $\hat{\mathbf{x}}$  satisfying  $d(\mathbf{x}, \hat{\mathbf{x}}) = 2$ . For example, we consider  $\mathbf{x}$  and  $\hat{\mathbf{x}}$  that have  $\theta = \{1, 2, \dots, K\}$ ,  $\hat{\theta} = \{1, 2, \dots, K-1, K+1\}$ ,  $\mathbf{c} = \hat{\mathbf{c}}$ , and  $s = \hat{s}$ . It is shown from this example that  $\beta_n = 0$  for  $n = 1, \dots, K-1$  and  $n = K+2, \dots, N$ , while  $\beta_K, \beta_{K+1} \neq 0$ , leading to  $d(\mathbf{x}, \hat{\mathbf{x}}) = 2$ .

*Remark 2:* The diversity order achieved by SS-SIM-OFDM in case of  $\theta \neq \hat{\theta}$  is two, which is far smaller than that attained in the first case with  $\theta = \hat{\theta}$ , especially when  $K$  increases. Obviously, the overall diversity order is  $G_d = 2$ . It is also noteworthy that the worst PEE occurs when  $\mathbf{x}$  and  $\hat{\mathbf{x}}$  have the same spreading code and  $M$ -ary symbol, and especially their active sub-carrier indices are identical at  $K-1$  positions. Such insights into the unbalance of the diversity gains attained in different domains motivate us to propose two methods to enhance the diversity gain  $G_d$  in the next section.

Finally, the theoretical upper bound on the BEP of the proposed scheme is expressed by

$$P_b \leq \frac{1}{2^p p} \sum_{\mathbf{x}} \sum_{\hat{\mathbf{x}}} P(\mathbf{x} \rightarrow \hat{\mathbf{x}}) w(\mathbf{x}, \hat{\mathbf{x}}), \quad (19)$$

where  $P(\mathbf{x} \rightarrow \hat{\mathbf{x}})$  is given in (15) and  $w(\mathbf{x}, \hat{\mathbf{x}})$  is the number of bit errors of the PEE of  $\mathbf{x} \rightarrow \hat{\mathbf{x}}$ .

## B. Diversity Enhancement

As analyzed in the previous section, the diversity order of SS-SIM-OFDM is always limited by two in the SI domain, regardless of increasing  $K$ . Moreover, unlike the existing IM schemes, the diversity gain of the proposed scheme strongly depends on the order of sub-carrier indices in each SI set  $\theta$ . For instance, when  $(N, K) = (3, 2)$ , we consider  $\mathcal{I}_1 = \{(1, 2), (2, 3)\}$  and  $\mathcal{I}_2 = \{(1, 2), (3, 2)\}$  which have the same elements in every SI set, but in different orders. The precoding vectors obtained by  $\mathcal{I}_1$ ,  $\mathcal{I}_2$  and  $\mathbf{c} = [c_1, c_2]^T$  are  $\mathcal{T}(\mathcal{I}_1, \mathbf{c}) = \{[c_1, c_2, 0]^T, [0, c_1, c_2]^T\}$  and  $\mathcal{T}(\mathcal{I}_2, \mathbf{c}) = \{[c_1, c_2, 0]^T, [0, c_2, c_1]^T\}$ . Because the Hamming distance between two precoding vectors in  $\mathcal{T}(\mathcal{I}_1, \mathbf{c})$  is larger than that in  $\mathcal{T}(\mathcal{I}_2, \mathbf{c})$ ,  $\mathcal{I}_1$  provides a better diversity gain than  $\mathcal{I}_2$ . Based on this insight, we propose two diversity enhancement methods for SS-SIM-OFDM as follows.

1) *Sub-carrier index set reduction (SISR):* This simple method is to reduce the number of SI sets  $\theta$  used in the SIM process. Although the SISR method suffers from the loss of the sub-carrier index bits, we can compensate this loss by increasing the  $M$ -ary modulation size. Let us give an example with  $(N, K) = (4, 3)$ . While the combinatorial method uses all possible 4 SI sets as  $\mathcal{I} = \{(1, 2, 3), (1, 2, 4), (1, 3, 4), (2, 3, 4)\}$ ,

the proposed SISR can employ either  $\mathcal{I} = \{(1, 2, 3), (2, 3, 4)\}$  or  $\mathcal{I} = \{(1, 2, 3), (2, 1, 4)\}$  to increase  $G_d$  from 2 to 3.

2) *Ordering Sub-carrier Indices (OSI):* Since existing IM schemes have the performance independent of the order of sub-carrier indices in each SI set  $\theta$ , they just simply employ the same descending or ascending order for all SI sets. However, such an ordering is not preferable for SS-SIM-OFDM. Particularly, the same order not only increases the number of the worst PEEs, but also limits the achievable diversity order of being two as shown in Remark 2. Thus, we propose the OSI method to improve the diversity gain of SS-SIM-OFDM, taking the order of sub-carrier indices into consideration.

We first derive the criteria for the OSI method in designing  $\mathcal{I} = \{\theta_1, \dots, \theta_{2^{p_1}}\}$  to maximize the diversity gain of SS-SIM-OFDM. For given two different SI sets  $\theta_m = \{\alpha_1, \dots, \alpha_K\}$  and  $\theta_n = \{\mu_1, \dots, \mu_K\}$  in  $\mathcal{I}$ , where  $m \neq n \in \{1, \dots, 2^{p_1}\}$ , denote by  $\Omega(\theta_m, \theta_n)$  the number of indices  $k \in \{1, \dots, K\}$  such that  $\alpha_k \neq \mu_k$ . Let  $\kappa = \min_{m \neq n} \Omega(\theta_m, \theta_n)$  and  $\Gamma = \sum_{n=1}^{2^{p_1}} \sum_{m \neq n=1}^{2^{p_1}} \Omega(\theta_m, \theta_n)$ . The OSI method is to design  $\mathcal{I}$  that maximizes  $\kappa$  first and then  $\Gamma$ . It can be seen that  $\Omega(\theta_m, \theta_n) \leq K$  for every  $m \neq n$ , thus  $\kappa \leq K$  and  $\Gamma \leq 2^{p_1} (2^{p_1} - 1) K$ . As a result, the best design of  $\mathcal{I}$  is the one that satisfies  $\Omega(m, n) = K$  for every  $m \neq n$ .

Based on the criteria above, the OSI method includes two following steps. The first step is to create  $\mathcal{I}_1 = \{\check{\theta}_1, \dots, \check{\theta}_{2^{p_1}}\}$  that satisfies the probabilities of indices  $i$  appearing in  $\mathcal{I}_1$  are the same for  $i = 1, \dots, N$ , without considering the order of sub-carrier indices. While the equiprobable sub-carrier activation (ESA) algorithm [37] can be used to carry out this step, we propose a simpler approach as follows. Rather than directly designing  $\mathcal{I}_1$  with  $2^{p_1}$  SI sets, we just need to design  $\mathcal{I}_2$  with  $T = C(N, K) - 2^{p_1}$  SI sets which also have the same property as  $\mathcal{I}_1$ . Then, the desired  $\mathcal{I}_1$  is determined by  $\mathcal{I}_1 = \mathcal{I}_0 - \mathcal{I}_2$ , where  $\mathcal{I}_0$  contains all  $C(N, K)$  possible SI sets. Since  $T \ll 2^{p_1}$ , designing  $\mathcal{I}_2$  is easier than  $\mathcal{I}_1$ . For example, when  $(N, K) = (4, 2)$  with  $2^{p_1} = 4$  and  $T = 2$ , we just simply pick up  $\mathcal{I}_2 = \{(1, 2), (3, 4)\}$  to obtain  $\mathcal{I}_1 = \mathcal{I}_0 - \mathcal{I}_2 = \{(1, 3), (1, 4), (2, 3), (2, 4)\}$ .

In the second step, utilizing  $\mathcal{I}_1$ , we design the OSI algorithm to reorder the indices of every SI set in  $\mathcal{I}_1$  to attain  $\mathcal{I} = \{\theta_1, \dots, \theta_{2^{p_1}}\}$  that fulfils the criteria of maximizing  $\kappa$  and  $\Gamma$ . Notice that maximizing  $\kappa$  is more important than  $\Gamma$  since  $\kappa$  is the main factor determining the diversity gain in the SI domain. The proposed OSI algorithm is described in Algorithm 3, where for each  $\check{\theta}_n \in \mathcal{I}_1$ , denote by  $\mathcal{F}(\check{\theta}_n) = \{\check{\theta}_n^{(1)}, \dots, \check{\theta}_n^{(L)}\}$  the set of all  $L = K!$  permutations of  $\check{\theta}_n$ . To better understand this algorithm, let us recall the example in the first step. Particularly, after conducting the OSI algorithm with the input  $\mathcal{I}_1$ , we attain the resulting  $\mathcal{I} = \{(1, 3), (4, 1), (3, 2), (2, 4)\}$  with  $\kappa = K = 2$ , and  $\Gamma = 2^{p_1} (2^{p_1} - 1) K = 24$ , while the combinatorial method results in  $\kappa = 1$  and  $\Gamma = 16$ .

It should be noted that unlike the SISR, the OSI method can significantly enhance the diversity gain of SS-SIM-OFDM without sacrificing the SE. This can be shown in Table I, which compares the diversity order when using the OSI and



**Algorithm 3** Ordering Sub-carrier Indices (OSI) Algorithm

**Input:**  $\mathcal{I}_1 = \{\ddot{\theta}_1, \dots, \ddot{\theta}_{2^{p_1}}\}$  obtained from the first step.

**Output:**  $\mathcal{I} = \{\theta_1, \dots, \theta_{2^{p_1}}\}$

- 1) Set  $\theta_1 = \ddot{\theta}_1$ .
- 2) **for**  $n = 2$  **to**  $2^{p_1}$  **do**
- 3) Set  $\theta_n = \ddot{\theta}_n^{(1)}$ .
- 4)  $\kappa_1 = \min_{l=1, \dots, n-1} \Omega(\ddot{\theta}_n^{(1)}, \theta_l)$ .
- 5) **for**  $m = 2$  **to**  $U$  **do**
- 6)  $\kappa_m = \min_{l=1, \dots, n-1} \Omega(\ddot{\theta}_n^{(m)}, \theta_l), \ddot{\theta}_n^{(m)} \in \mathcal{F}(\ddot{\theta}_n)$ .
- 7)  $\Gamma_m = \sum_{l=1}^{n-1} \Omega(\ddot{\theta}_n^{(m)}, \theta_l)$ .
- 8) **if**  $\kappa_m > \kappa_{m-1}$  **or**
- 9)  $\kappa_m = \kappa_{m-1}$  **and**  $\Gamma_m > \Gamma_{m-1}$
- 10) Set  $\theta_n = \ddot{\theta}_n^{(m)}$ .
- 11) **end if**
- 12) **end for**
- 13) **end for**

TABLE I

$G_d$  and  $N_d$  COMPARISON BETWEEN THE OSI AND COMBINATORIAL METHODS FOR VARIOUS VALUES OF  $(N, K)$

$(N, K)$	OSI		Comb	
	$G_d$	$N_d$	$G_d$	$N_d$
(3, 2)	2	6	2	8
(4, 2)	2	12	2	20
(5, 4)	4	80	2	12
(5, 3)	2	3	2	26

combinatorial methods for various  $(N, K)$  and  $M = 2$ . We also include the number of the worst PEEs (denoted by  $N_d$ ) whose PEPs have the diversity order of  $G_d$ . Note that in case two schemes have the same  $G_d$ , which one has smaller  $N_d$  would be better. As seen in Table I, the OSI method provides a significantly smaller  $N_d$  and larger  $G_d$  than the combinatorial method. Hence, the OSI method can remarkably reduce the BEP of SS-SIM-OFDM as validated in Section V.

## V. SIMULATION RESULTS

We present simulation results to verify the performance of SS-SIM-OFDM with various detectors and diversity enhancement methods. We select SS-OFDM-IM [33], ReMO [30], CI-OFDM-IM [28], classical OFDM-IM [6] and OFDM as benchmark schemes. For convenience, the configurations of SS-SIM-OFDM, ReMO, CI-OFDM-IM and OFDM-IM are represented by  $(N, K, M)$ , while that of SS-OFDM-IM is  $(N, M)$ , where  $M$  is the modulation size and  $N, K$  are numbers of sub-carriers and active ones per cluster, respectively. The PSK modulation is used for all the schemes. We summarize all simulation parameters of the proposed SS-SIM-OFDM scheme in Table II.

Fig. 3 depicts the BEP of SS-SIM-OFDM with various SI mapping methods such as the combinatorial [6], proposed SISR and OSI methods. For SISR, we employ a larger  $M$  than two remaining methods to make all of them have the same SE. Particularly,  $M = 4$  and 8 are used for SISR in Fig. 3(a) and Fig. 3(b), respectively. As seen from Fig. 3, the proposed SISR and OSI methods provide better BEP than the

TABLE II

A SUMMARY OF SIMULATION PARAMETERS OF SS-SIM-OFDM

Parameter	Value
Number of sub-carriers for each cluster $N$	4, 5
Modulation order $M$	2, 4, 8, 16
Number of active sub-carriers $K$	2, 3, 4
Spectral efficiency (bps/Hz)	1, 1.25, 1.5
Channel model	Rayleigh fading
$M$ -ary modulation type	PSK
CSI condition	Perfect, imperfect

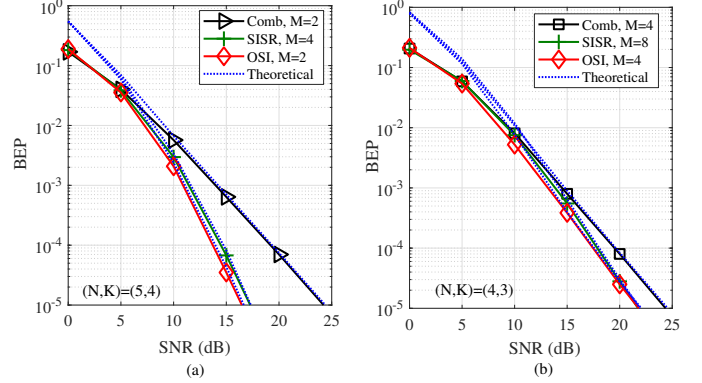


Fig. 3. BEP performance of SS-SIM-OFDM when different SI mapping methods are employed, and (a)  $(N, K) = (5, 4)$ ,  $M = 2$  or  $M = 4$  and (b)  $(N, K) = (4, 3)$ ,  $M = 4$  or  $M = 8$ .

combinatorial method, as both are designed to enhance the diversity gain of SS-SIM-OFDM. For instance, in Fig. 3(a), at  $\text{BEP} = 10^{-4}$ , there are respectively 5 and 5.5 dB SNR gains achieved by SISR and OSI over the combinatorial method. In addition, the theoretical bound is very tight, especially at high SNRs. Hence, the derived bound can be an effective tool to evaluate the BEP of the proposed scheme at high SNRs. Since OSI performs better than SISR, hereinafter, we will mainly use OSI in SS-SIM-OFDM for comparisons.

Fig. 4 compares the BEP performance between SS-SIM-OFDM and benchmark schemes with the ML detector at the SE of 1 bps/Hz. Obviously, the proposed scheme with either OSI or SISR significantly outperforms all benchmarks, especially at moderate and high SNRs. For example, at  $\text{BER} = 10^{-4}$  in Fig. 4, SS-SIM-OFDM employing OSI exhibits 3, 5, 6, 15, 21 dB SNR gains over SS-OFDM-IM, ReMO, CI-OFDM-IM, OFDM-IM and OFDM, respectively. This performance gain comes from the fact that our scheme is designed specifically to provide higher diversity gain than the benchmarks, whose gain is often limited by two. The same observation can be found in Fig. 5 with a SE of 1.25 bps/Hz.

In Fig. 6, we show the BEP comparison between the proposed and benchmark schemes at the SE of 1.5 bps/Hz. Once again, our scheme is superior to all benchmarks in terms of the BEP performance in a wide range of SNRs. Specifically, at  $\text{BEP} = 10^{-3}$  in Fig. 6, SS-SIM-OFDM of  $(4, 3, 4)$  outperforms SS-OFDM-IM, ReMO, CI-OFDM-IM and OFDM-IM with SNR gains of 2, 2.5, 4 and 8 dB, respectively. Therefore, we can conclude that our SS-SIM-OFDM provides higher reliability than the benchmark schemes, especially at low SEs.

Fig. 7 presents the BEP comparison between the proposed

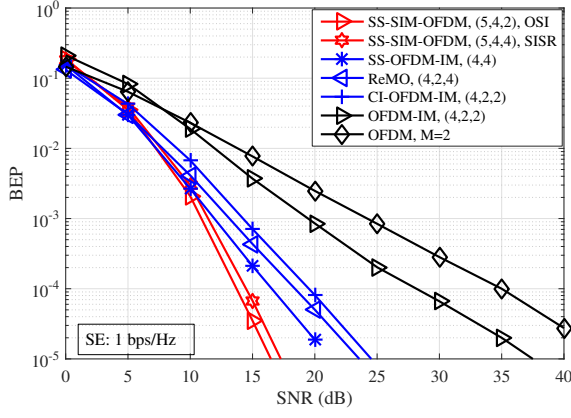


Fig. 4. BEP comparison among SS-SIM-OFDM and benchmark schemes at the SE of 1 bps/Hz. The ML detection is used.

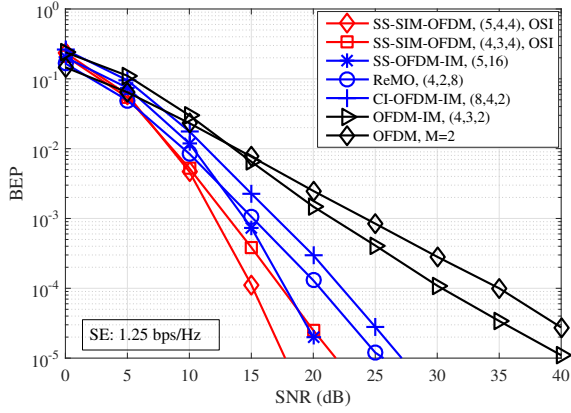


Fig. 5. BEP comparison among SS-SIM-OFDM and benchmark schemes at the SE of 1.25 bps/Hz. All schemes use the ML detector.

near-ML, LLR-MRC detectors and the ML detector when  $(N, K) = (4, 2)$  and  $M = \{4, 16\}$ , under both perfect and imperfect CSI conditions. Here, we consider the CSI uncertainty caused by the minimum mean square error estimator [7]. It is shown from Fig. 7 that the proposed near-ML achieves a near-optimal BEP as the ML detector, while the LLR-MRC detector suffers from the performance loss, particularly when  $M$  is small, i.e.,  $M = 4$ . This is due to the fact that when the modulation order  $M$  is small, the performance of LLR-MRC is more influenced by the index detection error than by the  $M$ -ary symbol detection error. More particularly, in order to achieve the lowest complexity, LLR-MRC has to detect the indices of active sub-carriers first, which makes it more sensitive to the index detection error than the ML and near-ML detectors that jointly detect both the active indices and  $M$ -ary symbol. Finally, the gap between LLR-MRC and ML or near-ML becomes negligible when  $M$  increases or the CSI is imperfect, as shown in Fig. 7(b). As a result, our detectors are appropriate for practical implementations of SS-SIM-OFDM.

## VI. CONCLUSION

We have proposed a novel IM scheme called as SS-SIM-OFDM to improve the reliability of existing IM-based systems. In SS-SIM-OFDM, SS and SI modulations are jointly employed

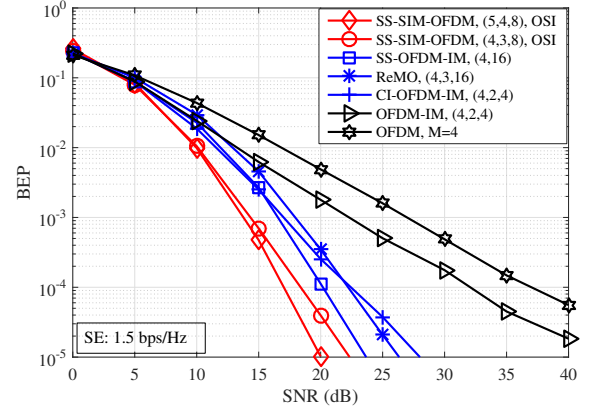


Fig. 6. BEP comparison among SS-SIM-OFDM and benchmark schemes at the SE of 1.5 bps/Hz and the ML detector is used for all schemes.

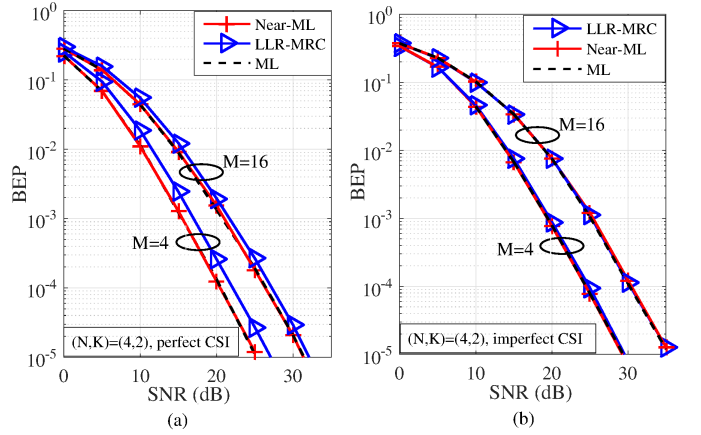


Fig. 7. BEP comparison between our near-ML and LLR-MRC detectors and the ML detector, under (a) perfect and (b) imperfect CSI, when  $(N, K) = (4, 2)$  and  $M = \{4, 16\}$ . The OSI method is used for our scheme.

to form a precoding vector which is then used to spread an  $M$ -ary modulated symbol across all active sub-carriers. As a result, all three possible signal dimensions of the existing IM schemes, including indices of both spreading codes and sub-carriers, and the  $M$ -ary symbol are exploited to convey data bits. We designed two reduced-complexity detectors, namely the near-ML and LLR-MRC detectors, whose complexities are roughly independent of the modulation size. Then, the BEP and its upper bound were derived to gain an insight into the diversity gain. Based on this, two diversity enhancement methods, namely SISR and OSI, were proposed, in which OSI can significantly improve the diversity gain without losing the SE, while SISR suffers from the decrease of SI bits. Simulation results showed that our scheme employing SISR and OSI achieves lower BEP than the benchmarks. In addition, the near-ML detector achieves the optimal BEP, while the LLR-MRC detector having lowest complexity suffers from a slight performance loss. However, the performance gap between two detectors becomes marginal when  $M$  increases or the CSI is imperfect. Our future work will focus on increasing the SE of SS-SIM-OFDM through transmitting multiple  $M$ -ary symbols such that it can perform well at higher SEs.



## REFERENCES

- [1] E. Basar, M. Wen, R. Mesleh, M. D. Renzo, Y. Xiao, and H. Haas, "Index modulation techniques for next-generation wireless networks," *IEEE Access*, vol. 5, pp. 16693–16746, 2017.
- [2] R. Y. Mesleh, H. Haas, S. Sinanovic, C. W. Ahn, and S. Yun, "Spatial modulation," *IEEE Trans. Veh. Technol.*, vol. 57, no. 4, pp. 2228–2241, July 2008.
- [3] G. Kaddoum, M. F. A. Ahmed, and Y. Nijssure, "Code index modulation: A high data rate and energy efficient communication system," *IEEE Commun. Lett.*, vol. 19, no. 2, pp. 175–178, Feb 2015.
- [4] P. K. Frenger and N. A. B. Svensson, "Parallel combinatory OFDM signaling," *IEEE Trans. Commun.*, vol. 47, no. 4, pp. 558–567, Apr 1999.
- [5] C. Bockelmann, N. Pratas, H. Nikopour, K. Au, T. Svensson, C. Stefanovic, P. Popovski, and A. Dekorsy, "Massive machine-type communications in 5G: physical and MAC-layer solutions," *IEEE Commun. Mag.*, vol. 54, no. 9, pp. 59–65, 2016.
- [6] E. Basar, U. Aygolu, E. Panayirci, and H. V. Poor, "Orthogonal frequency division multiplexing with index modulation," *IEEE Trans. Signal Process.*, vol. 61, no. 22, pp. 5536–5549, Nov 2013.
- [7] T. V. Luong and Y. Ko, "Impact of CSI uncertainty on MCIC-OFDM: tight, closed-form symbol error probability analysis," *IEEE Trans. Veh. Technol.*, vol. 67, no. 2, pp. 1272 – 1279, Feb 2018.
- [8] M. Wen, X. Cheng, M. Ma, B. Jiao, and H. V. Poor, "On the achievable rate of OFDM with index modulation," *IEEE Trans. Signal Process.*, vol. 64, no. 8, pp. 1919–1932, April 2016.
- [9] T. V. Luong and Y. Ko, "Symbol error outage performance analysis of MCIC-OFDM over complex TWDP fading," in *Proc. Eur. Wireless*, May 2017, pp. 1–5.
- [10] R. Fan, Y. J. Yu, and Y. L. Guan, "Generalization of orthogonal frequency division multiplexing with index modulation," *IEEE Trans. Wireless Commun.*, vol. 14, no. 10, pp. 5350–5359, Oct 2015.
- [11] T. Mao, Z. Wang, Q. Wang, S. Chen, and L. Hanzo, "Dual-mode index modulation aided OFDM," *IEEE Access*, vol. 5, pp. 50–60, 2017.
- [12] M. Wen, E. Basar, Q. Li, B. Zheng, and M. Zhang, "Multiple-mode orthogonal frequency division multiplexing with index modulation," *IEEE Trans. Commun.*, vol. 65, no. 9, pp. 3892–3906, Sept 2017.
- [13] M. Wang, Z. Chen, and Z. Chen, "Dual-mode index modulation aided 3D-OFDM," *IEEE Commun. Lett.*, vol. 26, no. 3, pp. 612–616, 2022.
- [14] J. Choi, "Noncoherent OFDM-IM and its performance analysis," *IEEE Transactions on Wireless Communications*, vol. 17, no. 1, pp. 352–360, Jan 2018.
- [15] T. Van Luong, Y. Ko, N. A. Vien, M. Matthaiou, and H. Q. Ngo, "Deep energy autoencoder for noncoherent multicarrier MU-SIMO systems," *IEEE Trans. Wireless Commun.*, vol. 19, no. 6, pp. 3952–3962, 2020.
- [16] A. Fazeli, H. H. Nguyen, H. D. Tuan, and H. V. Poor, "Non-coherent multi-level index modulation," *IEEE Trans. Commun.*, vol. 70, no. 4, pp. 2240–2255, 2022.
- [17] D. Feng, J. Zheng, B. Bai, J. Jiang, and L. Zheng, "In-phase and quadrature index modulation aided OTFS transmission," *IEEE Commun. Lett.*, pp. 1–1, 2022.
- [18] H. Zhang, D. Kong, Y. Xin, L. Xiao, and T. Jiang, "Filter bank orthogonal frequency division multiplexing with index modulation," *IEEE Commun. Lett.*, vol. 25, no. 12, pp. 3960–3964, 2021.
- [19] T. V. Luong, Y. Ko, N. A. Vien, D. H. N. Nguyen, and M. Matthaiou, "Deep learning-based detector for OFDM-IM," *IEEE Wireless Commun. Lett.*, vol. 8, no. 4, pp. 1159–1162, Aug. 2019.
- [20] T. Wang, F. Yang, J. Song, and Z. Han, "Deep convolutional neural network-based detector for index modulation," *IEEE Wireless Commun. Lett.*, vol. 9, no. 10, pp. 1705–1709, 2020.
- [21] T. Van Luong, X. Zhang, L. Xiang, T. M. Hoang, C. Xu, P. Petropoulos, and L. Hanzo, "Deep learning-aided optical IM/DD OFDM approaches the throughput of RF-OFDM," *IEEE J. Sel. Areas Commun.*, vol. 40, no. 1, pp. 212–226, 2022.
- [22] X. Zhang, T. Van Luong, P. Petropoulos, and L. Hanzo, "Machine-learning-aided optical OFDM for intensity modulated direct detection," *J. Lightw. Technol.*, vol. 40, no. 8, pp. 2357–2369, 2022.
- [23] T. V. Luong, Y. Ko, M. Matthaiou, N. A. Vien, M.-T. Le, and V.-D. Ngo, "Deep learning-aided multicarrier systems," *IEEE Trans. Wireless Commun.*, vol. 20, no. 3, pp. 2109–2119, 2021.
- [24] C. Xu, T. Van Luong, L. Xiang, S. Sugiura, R. G. Maunder, L.-L. Yang, and L. Hanzo, "Turbo detection aided autoencoder for multi-carrier wireless systems: Integrating deep learning into channel coded systems," *IEEE Trans. Cogn. Commun. Netw.*, pp. 1–1, 2022.
- [25] E. Basar, "On multiple-input multiple-output OFDM with index modulation for next generation wireless networks," *IEEE Trans. Signal Process.*, vol. 64, no. 15, pp. 3868–3878, Aug 2016.
- [26] J. Crawford, E. Chatziantoniou, and Y. Ko, "On the SEP analysis of OFDM index modulation with hybrid low complexity greedy detection and diversity reception," *IEEE Trans. Veh. Technol.*, vol. 66, no. 9, pp. 8103–8118, Sept 2017.
- [27] T. V. Luong and Y. Ko, "The BER analysis of MRC-aided greedy detection for OFDM-IM in presence of uncertain CSI," *IEEE Wireless Commun. Lett.*, vol. 7, no. 4, pp. 566–569, 2018.
- [28] E. Basar, "OFDM with index modulation using coordinate interleaving," *IEEE Wireless Commun. Lett.*, vol. 4, no. 4, pp. 381–384, Aug 2015.
- [29] M. Wen, B. Ye, E. Basar, Q. Li, and F. Ji, "Enhanced orthogonal frequency division multiplexing with index modulation," *IEEE Trans. Wireless Commun.*, vol. 16, no. 7, pp. 4786 – 4801, July 2017.
- [30] T. V. Luong, Y. Ko, and J. Choi, "Repeated MCIC-OFDM with enhanced transmit diversity under CSI uncertainty," *IEEE Trans. Wireless Commun.*, vol. 17, no. 6, pp. 4079–4088, June 2018.
- [31] J. Choi, "Coded OFDM-IM with transmit diversity," *IEEE Trans. Commun.*, vol. 65, no. 7, pp. 3164–3171, July 2017.
- [32] T. T. H. Le, X. N. Tran, V.-D. Ngo, and M.-T. Le, "Repeated index modulation-OFDM with coordinate interleaving: Performance optimization and low-complexity detectors," *IEEE Syst. J.*, pp. 1–9, 2020.
- [33] Q. Li, M. Wen, E. Basar, and F. Chen, "Index modulated OFDM spread spectrum," *IEEE Trans. Wireless Commun.*, vol. 17, no. 4, pp. 2360–2374, 2018.
- [34] T. V. Luong and Y. Ko, "Spread OFDM-IM with precoding matrix and low-complexity detection designs," *IEEE Trans. Veh. Technol.*, vol. 67, no. 12, pp. 11 619–11 626, Dec. 2018.
- [35] C. Xu, Y. Xiong, N. Ishikawa, R. Rajashekar, S. Sugiura, Z. Wang, S.-X. Ng, L.-L. Yang, and L. Hanzo, "Space-, time- and frequency-domain index modulation for next-generation wireless: A unified single-/multi-carrier and single-/multi-RF MIMO framework," *IEEE Trans. Wireless Commun.*, vol. 20, no. 6, pp. 3847–3864, 2021.
- [36] M. K. Simon and M. S. Alouini, *Digital Communication over Fading Channels*. 2nd edition. John & Wiley, 2005.
- [37] M. Wen, Y. Zhang, J. Li, E. Basar, and F. Chen, "Equiprobable subcarrier activation method for OFDM with index modulation," *IEEE Commun. Lett.*, vol. 20, no. 12, pp. 2386–2389, Dec 2016.